RSC Advances




ROYAL SOCIETY OF CHEMISTRY

www.rsc.org/advances

# Role of substrate effects on the morphological, structural, electrical and thermoelectrical properties of $V_2O_5$ thin films.

Bilal Ahmad[1], G.R. Khan[1*], and K. Asokan[2*]
[1]*Nanotechonology Research Lab, Department of Physics, National Institute of Technology Hazratbal Srinagar, J & K-190006, India.*
[2]*Materials Science Division, Inter University Accelerator Centre, Aruna Asaf Ali Marg, New Delhi-110067, India.*

## Abstract

Present work focuses on the influence of different substrates on the morphological, compositional, phase purity, structural and transport properties of vanadium pentaoxide ($V_2O_5$) thin films. Thin films of $V_2O_5$ were fabricated on different substrates: glass, quartz, Si, and alumina, (hereafter these films are refereed as $V_2O_5$:G, $V_2O_5$:Q, $V_2O_5$:Si and $V_2O_5$:A respectively), using inorganic sol gel with $V_2O_5$ power and hydrogen peroxide ($H_2O_2$) as precursors by spin coater. Films deposited on glass substrates were found to be amorphous in nature with smooth surfaces, whereas films deposited on quartz, silicon, and alumina substrates exhibited polycrystalline nature having orthorhombic structure with space group Pmmn. The crystallinity improves from quartz to silicon and best crystalline films were fabricated on alumina. Electrical measurements as a function of temperature and substrate are investigated and characterized by measuring the resistivity, Hall and Seebeck coefficients. Negative values of Hall and Seebeck coefficients reveal that all the films are of n-type semiconductors. Electrical resistivity as well as charge carrier density decreases from the films on glass to quartz to silicon and to alumina. Carrier mobility decreases in the following order $V_2O_5$:G > $V_2O_5$:A >$V_2O_5$:Si> $V_2O_5$:Q, where as Seebeck coefficient varies in the reverse order. Variation of these transport parameters has been understood on the basis of scattering and trapping of charge carriers along the grain boundaries. Further a model based on thermodynamics is proposed to explain the effect of substrates on crystallinity of thin films. Interactions between sol and substrate (adhesive forces) are determined by the thickness, phase purity, structural and morphological properties of thin films. As the magnitude of adhesive forces increases, both film thickness as well as crystallinity increases.

*Corresponding authors

## 1. Introduction

Vanadium oxides offer many convenient physical effects which can be used for different microelectronic device applications [1]. Vanadium is a multivalent element and as a result forms variety of oxides upon reacting with oxygen such as VO, $V_2O_3$, $VO_2$, $V_6O_{11}$, $V_2O_5$ etc. $V_2O_5$ is the saturated (highest oxidation state) in the V-O system and consequently the most stable one among these vanadium oxides [2-3]. It has a lamellar, or sheet like structure [4]. It is a distorted orthorhombic structure, and this deformation creates its sheet formation. $V_2O_5$ in the form of thin films has attracted much attention due to its unique electronic, chemical and optical properties [5-8]. Thin films of $V_2O_5$ have been prepared by different techniques including: vacuum evaporation [9], sputter deposition [10-13], thermal oxidation [14-15], pulsed laser deposition [16],chemical vapor deposition [17-19], sol-gel processes [20] and spray pyrolysis [21]. Due to the advantages of high purity, homogeneity, stoichiometry, simplicity of equipments involved and cost effectiveness for large scale production, the sol gel process has become one of the best approaches to deposit metal oxide thin films.

Recently, it was reported that the metal to insulator transition (MIT) at approximately 280°C in $V_2O_5$ is due to lattice distortion and a structural inhomogeneity due to the vanadyl-oxygen vacancies [22–24] and this makes $V_2O_5$ a promising material for thermoelectric devices. $V_2O_5$ exhibits highly anisotropic electrical and optical properties due to its orthorhombic structure [25] and these properties have been extensively investigated by many researchers [25-28]. On the other hand, the thermo-physical properties including thermal conductivity (κ), Seebeck coefficient (s), and dynamic heat capacity have received less attention [29-31]. One of the important parameters for characterizing the thermo-physical properties of materials is a power factor ($s^2/\rho$), where $s$ the thermoelectric power (Seebeck coefficient), $\rho$ is the electrical resistivity. Thus to be a better thermoelectric material, a large value for $s$, and small values of $\rho$ are required. Surprisingly, the s and electrical resistivity ($\rho$) vary in a opposite way, preventing power factor from an excellent improvement, and both the values are also dependent on each other with carrier density (n). Generally, the s value of a semiconductor or an insulator decreases with increasing temperature. The variation of s with temperature is very important for thermoelectric applications.

In the present work, we investigate the effect of substrates on the microstructural evolution, crystal phase, and surface morphology, electrical and thermo-electrical properties of $V_2O_5$ thin films fabricated by sol-gel method. Crystallite size, surface morphology and film thickness were observed to vary from substrate to substrate which in turn affects the transport properties of thin films.

## 2. Experimental details

Clear yellow solution, containing 0.3 grams of $V_20_5$ (Sigma Aldrich, purity >99.9 %) dissolved in 30 ml, 30% hydrogen peroxide $H_2O_2$ (Sigma Aldrich), was formed at room temperature with vigorous stirring. This yellow solution was then heated at 60 $^0$C with continuous stirring to evolve excess oxygen by decomposition of $H_2O_2$. Immediately, the solution turned into red brown viscous gel. After aging for 24 hours, the $V_2O_5$ gel was ready for coating. The mechanism of reaction is given in reactions (A) and (B) following Ren et al. [32].

$$V_2O_5 + 2H_2O_2 \longrightarrow 2HVO_4 + H_2O \qquad (A)$$

$$2HVO_4 + (n-1)\,H_2O \longrightarrow V_2O_5.\,nH_20 + O_2 \qquad (B)$$

The spin coater (Spin-NXG-P1: made by Apex Instruments, India) was used to deposit thin films on glass, quartz, Si, and alumina substrates. Prior to deposition, these substrates were cleaned in dilute sulphuric acid for 30 minutes and then thoroughly rinsed with ethanol, acetone and de-ionized water. Five coatings of $V_2O_5$ gel were performed on each substrate with the rate of 3000 rpm for 30 seconds and after each coating the films were dried at 80$^0$C for 15-20 minutes. Finally these $V_2O_5$ gel films were crystallized by annealing at 400 $^0$C for 4 hours in the ambient atmosphere in programmable tubular furnace (Nabertherm GmbH Tube furnace: RHTC80) with heating and cooling rate of 3$^o$C per minute. Rutherford backscattering (RBS) with $He^+$ ions of energy 2 MeV was used to characterize stoichiometry, thickness and uniformity of the films. X-ray diffraction (XRD) measurements at room temperature in the 2θ range of 20–60$^o$ was performed to identify the crystalline phases and structure of the films using a Bruker D8 advance diffractometer with Cu Kα (0.15406 nm) X-ray source at a scan speed of 0.5$^o$/min. Raman studies of these films were carried out and the spectra were measured in back scattering geometry using an Ar excitation source having a wavelength of 488 nm coupled with a Labram-HR800 micro- Raman spectrometer equipped with a 50X objective, appropriate notch filter, and a Peltier cooled charge-coupled device detector. The surface morphology of films was

characterized by SEM (Model: MIRA II LMH, TESCAN). The electrical resistivity, Seebeck coefficients of the films were measured in the temperature range (300-400K) using a standard DC four probe technique and bridge method respectively. The Hall Effect measurements were carried out in the same temperature range by Ecopia HMS-3000 Hall Measurement System to evaluate charge carrier density and mobility.

## 3. RESULTS AND DISCUSSION

### 3.1. Morphological studies

Figure 1 shows the surface morphology of $V_2O_5$ thin films deposited on glass, quartz, Si, and alumina substrates investigated by SEM and these films hereafter will be referred as $V_2O_5$ :G, $V_2O_5$:Q, $V_2O_5$:Si, and $V_2O_5$:A respectively. As evident there is a significant change in the surface morphologies. Film deposited on glass substrate have relatively smooth surfaces with few compact structures revealing amorphous nature of the film and also some cracks are observed on the surface of this film which may be due to shrinkage of sol during the annealing of the film. Films deposited on quartz posses irregular nanostructures with varying sizes. The bigger particles grow due to agglomeration of smaller ones to reduce the surface energy under a thermodynamic driving force when two particles merge at high temperature. Surface of films deposited on Si and alumina posses cubic growth characteristics resembling a spiral like features which may have emanated from screw dislocations. The average crystallite size was found to be increased while moving from quartz through silicon to alumina. Further grain size distribution was found to be more random for $V_2O_5$ films deposited on quartz than those deposited on silicon and alumina substrates. This may be due to the difference in sticking coefficients and strains developed in the films grown on amorphous background. The average grain sizes of $V_2O_5$:Q, $V_2O_5$:Si and $V_2O_5$:A is approximately about 70nm, 135nm and 180 nm respectively. Larger grain size was observed in $V_2O_5$:A compared to $V_2O_5$:Si due to lattice mismatches of $V_2O_5$ and $Al_2O_3$ then $V_2O_5$ and Si.

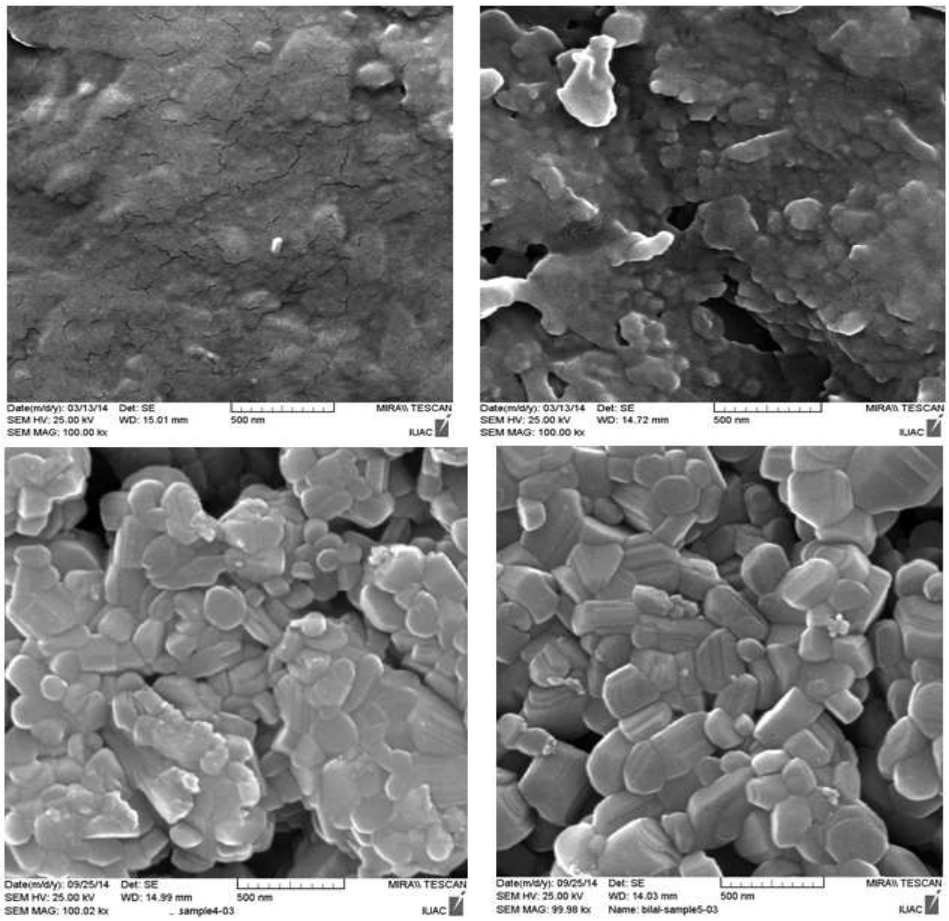


Figure 1:- SEM images of (a) $V_2O_5$: G (b) $V_2O_5$: Q (c) $V_2O_5$: Si and (d) $V_2O_5$: A. Films deposited on glass are amorphous in nature with smooth surfaces. Films deposited on quartz, Si and alumina are crystalline in nature and average crystallite size increases from quartz to Si and to alumina.

### 3.2. Compositional analysis

As mentioned above, oxides of vanadium can exist in a wide range of stoichiometries. The RBS measurements with SIMNRA Program were used to determine composition and thickness of films. RBS spectra (with SIMNRA simulation) of the four samples ($V_2O_5$:G, $V_2O_5$:Q, $V_2O_5$:Si, and $V_2O_5$:A) are shown in Figure 2 (a), (b), (c) and (d) respectively. The simulated results are summarized in the Table 1. This simulation suggests that the V/O ratios for all the samples are 2/5 within simulation errors indicating good stoichiometries of all these four thin films. Thickness was found to be ~ 46.7 nm, 85.5, 118.4 and 130.3nm for the films $V_2O_5$:G, $V_2O_5$:Q, $V_2O_5$:Si, $V_2O_5$:A respectively. Increase in film thickness from glass to quartz to Si to alumina may be due to increase of magnitude of cohesive forces in comparison to adhesive forces from $V_2O_5$:G, $V_2O_5$:Q, $V_2O_5$:Si, and $V_2O_5$:A. It is also clear that the RBS results indicated that there was no contamination during the film deposition.

**Table 1 Simulation results on composition of thin films on various substrates**

| Substrates | composition of film | | Thickness (nm) |
|---|---|---|---|
| | V | O | |
| Glass | 0.286 | 0.714 | 46.7 |
| Quartz | 0.286 | 0.714 | 85.5 |
| Si | 0.286 | 0.714 | 118.4 |
| Alumina | 0.286 | 0. 714 | 130.3 |

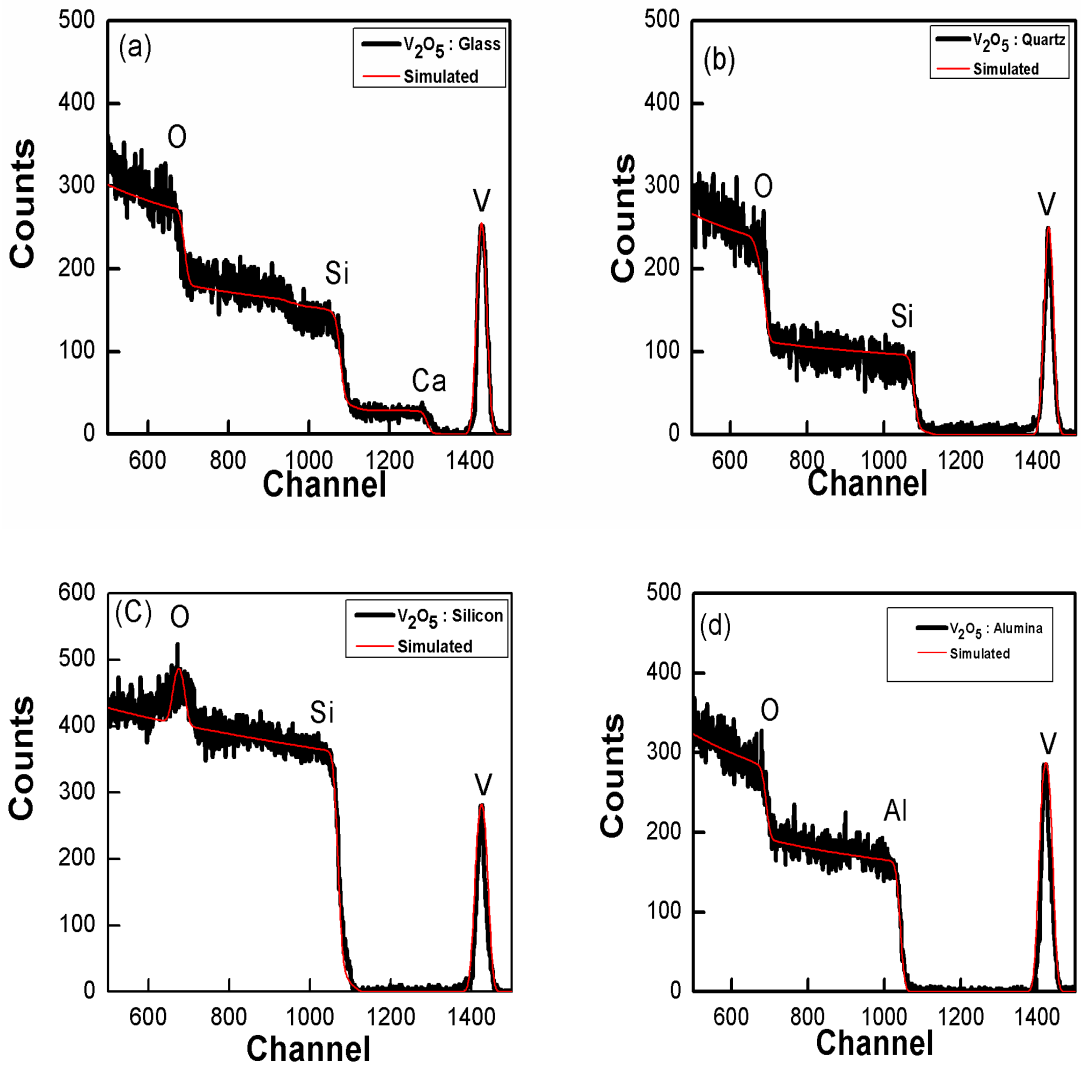


Figure 2:- RBS Spectra of (a) $V_2O_5$:G, (b) $V_2O_5$:Q, (c) $V_2O_5$: Si, and (d) $V_2O_5$:A. Thickness of film increases from glass (46.7 nm) to quartz (85.5nm) to silicon (118.4) to alumina (130.3 nm).

### 3.3. Phase Study

Figure 3 shows the XRD pattern of the $V_2O_5$ thin films deposited on glass, quartz, Si, and alumina substrates. The X-ray diffraction spectrum of $V_2O_5$ films deposited on glass substrate indicates amorphous nature as diffraction pattern is diffused and non characteristic. Films fabricated on quartz, Si, and alumina substrates are comprised of $V_2O_5$ phase within detection limit of XRD without any other phases of vanadium oxide. Intensity of diffraction peaks demonstrate that crystallinity increases from quartz through Si to alumina. Peaks are indexed according to standard pattern [JCPDS file no. 85-0601] for polycrystalline orthorhombic $V_2O_5$. The relative high intensity of the (001) peaks demonstrates the growth of films oriented along the c-axis perpendicular to the surface of substrate. In addition to (001) Bragg reflection, the subsequent appearance of other characteristic orientations such as (101), (110) and (002) reveals the existence of in-plane organization of V-O-V chains. The evaluated lattice parameters on the basis of measured d spacings for films on quartz, Si, and alumina are found to be $a = 0.3564 \pm 0.001$, $b = 1.151 \pm 0.001$, and $c = 0.433 \pm 0.001$ nm, these are in good agreement with previous, reported values in the literature [33]. Even though the (001) peak is the strongest in a polycrystalline XRD powder pattern of $V_2O_5$, the intensity ratios (I(001)/I(hkl)) in the sol-gel prepared films is larger than in polycrystalline $V_2O_5$ powder, indicating a strong (001) texture. This preferred orientation in the sol-gel films can be understood from the properties of the starting material. The gel is formed due to the hydrolysis and condensation of molecular precursors. The chemical control of these reactions allows the formation of $V_2O_5$ gels directly from the solutions at lower temperature than by standard solid state process [33-35]. Therefore, the sol-gel films are comprised of $V_2O_5.nH_2O$, before annealing at 400 C [37]. These have a $V_2O_5$ layered structure with trapped water molecules and are characterized by a strong structural anisotropy.

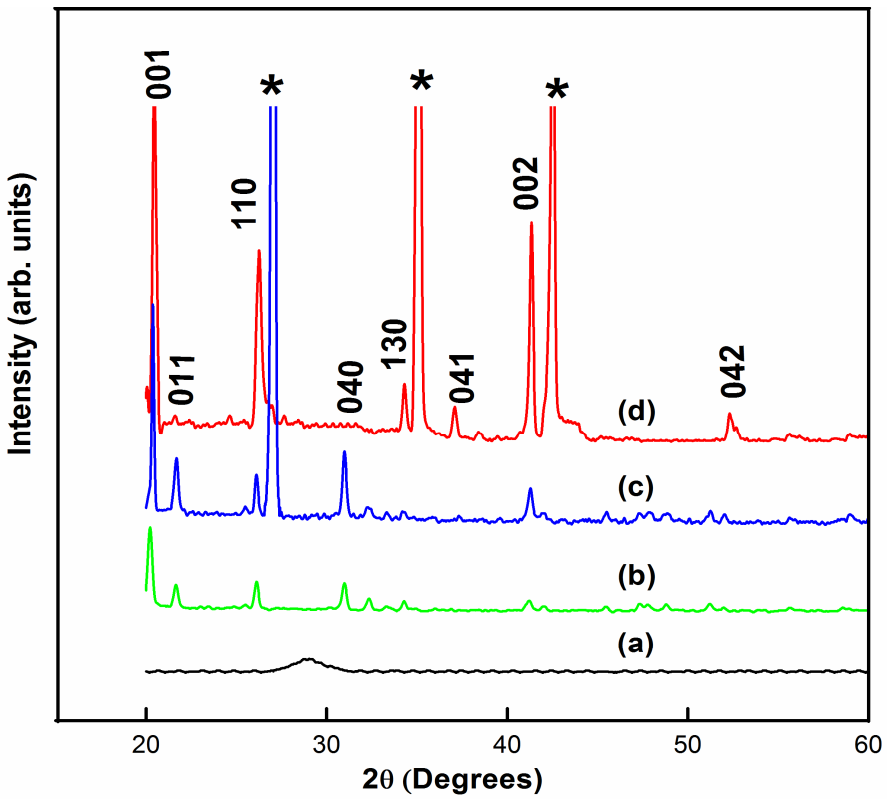


Figure 3:- XRD Spectra of (a) $V_2O_5$:G, (b) $V_2O_5$:Q, (c) $V_2O_5$:Si, and (d) $V_2O_5$:A. The '*' indexed peaks correspond to substrates.

### 3.4. Raman measurements

Figure 4 displays the Raman spectra of $V_2O_5$ thin films fabricated on glass, quartz, silicon, and alumina substrates in the wavelength range of 100-1100 $cm^{-1}$. The broad and non-characteristic Raman spectrum reveals the amorphous nature of $V_2O_5$ when deposited on glass substrate. The Raman spectra of films deposited on quartz, silicon and alumina substrates exhibit distinguishable and characteristic assignable Raman peaks indicating polycrystalline nature of these films. Peak intensities clearly demonstrate that crystallinity increases from films fabricated on quartz through silicon to alumina. Raman measurements of the films can be described using the shape and frequency of peaks.

$V_2O_5$ crystallizes in the orthorhombic system with the group $P_{mmn}(D_{2h}^{13})$ according to Bachmann et al. [32]. The structure of $V_2O_5$ is built up from $VO_5$ square pyramids sharing edges to form $(V_2O_4)_n$ zigzag double chains along [001] and cross linked along [100] by corner sharing and thus forming sheets in the xz plane [37-38]. Thus in each layer V is five-fold coordinated;

with three V-O bonds involving three fold coordinated oxygen ($O_c$) belonging to $(V_2O_4)_n$ chains, one V-O bond involving two fold coordinated oxygen($O_B$) constituting bridges between two chains and one involving vanadyl oxygen ($O_v$). The successive layers are kept together by an equal number of weak Vander Waals bonds and much stronger double bonds [39]. The unit cell contains two formula units ($V_4O_{10}$) yielding a total number of 39 optical zone centers. Due to the inversion symmetry and according to $D_{2h}$ factor group analysis, the modes split into IR (odd) and Raman (even) active modes. All the 21 g modes are Raman active while 15 $B_u$ modes are IR active. Beattie and Gilson [40] indicated that a convenient way to describe vibrations in binary oxide lattice is to treat oxygen atom as vibrating against an array of immobile metal atoms. Each oxygen species is then considered first as vibrating according to its site symmetry and, following this, the unit cell modes are generated by symmetry operations.

Table 2 depicts principal Raman active modes with corresponding motion of $V_2O_5$ thin films. Each spectrum consists of two groups of peaks located at high-frequency region known as internal modes and at low frequency region known as external modes. The internal modes that are observed in high frequency region are assigned to stretching and bending of V-O bonds. The high-frequency Raman peak at 1,006 $cm^{-1}$ gives the structural quality of the films and can be ascribed to the stretching mode related to the $A_g$ symmetry vibrations of the shortest vanadium oxygen bond which is $V{=}O_V$). Unlike the other O atoms this atom is strongly bonded to only one V atom and for this reason is called terminal oxygen [41]. The frequency shift of this mode measures the deviations from stoichiometry. The frequency shift to lower values of this mode is due to softening of the $V^{5+}{=}O$ bond in oxygen deficient $V_2O_5$ films resulting from vacancies created by removing $O_v$ with some of the $V^{5+}$ reduced to $V^{4+}$ for charge balance. Negligible frequency shift of this mode to the value 995 $cm^{-1}$ demonstrate good stoichiometry of all the three crystalline samples which is in good agreement with RBS and XRD results. This is also evident as no peak corresponding to $V^{4+}{=}O$ near 932 $cm^{-1}$ is observed as reported by Lee et al. [42]. The second peak at 702 $cm^{-1}$ is assigned to the doubly coordinated oxygen ($V_2$-$O_B$) stretching mode which results from corner-shared oxygen common to two pyramids. The third peak at 529 $cm^{-1}$ is assigned to the triply coordinated oxygen ($V_3$-$O_C$) stretching mode which results from edged-shared oxygen atoms common to three pyramids. The two peaks located at 404 and 283 $cm^{-1}$ are assigned to the bending vibration of the $V{=}O_V$ bonds. The peaks located at

481 $cm^{-1}$ and 304 $cm^{-1}$ is assigned to the bending vibrations of the bridging V-$O_B$-V (doubly coordinated oxygen) and $V_3$-O (triply coordinated oxygen) bonds, respectively.

The external modes can be viewed as relative motions of structural units with respect to each other, i.e. translations $T_x^1, T_y^1, T_z^1$ and librations $R_x^1, R_y^1, R_z^1$. These vibrations occur at low frequencies because each unit is considered heavier than constituent atoms while the restoring force has the same order of magnitude [43]. The external low frequency Raman modes at, 146 and 198 $cm^{-1}$ correspond to the relative motions of $V_2O_5$ layers with respect to each other [42]. These two peaks at 146$cm^{-1}$ and 198 $cm^{-1}$ are strongly associated with the layered structure and only appear when there is long range structural order. The presence of these low frequency modes in the films deposited on quartz, silicon and alumina substrates suggest that these films posses a layered structure and are well crystallized. The films grow preferentially with c-axis oriented perpendicular to the substrate plane [44].

**Table 2:-Raman active modes of orthorhombic $V_2O_5$ thin film.**

Symmetry and assignation of modes are mainly based on refs. [42-43]. Frequency values are derived from present measurements.

| Wave number ($cm^{-1}$) | Symmetry | Assignment | Remarks |
|---|---|---|---|
| 146 | $B_{3g}$, $B_{2g}$ | Ty, Rz | Relative motions of $V_2O_5$ layers with respect to each other. |
| 198 | $B_{1g}$ | Tx, Ry | Relative motions of $V_2O_5$ layers with respect to each other. |
| 283 | $B_{2g}$, $B_{3g}$ | δ(V=O)b. | Bending vibration of the V=$O_V$ bonds. |
| 304 | $A_g$ | δ(V3-O)b | Bending vibrations of the $V_3$-O (triply coordinated oxygen) bond |
| 404 | $A_g$ | δ(V=O)b | Bending vibration of the V=$O_V$ bonds. |
| 481 | $A_g$ | δ(V-O-V)b | Bending vibrations of the bridging V-$O_B$-V (doubly coordinated oxygen) |
| 529 | $A_g$ | ν(V3-O)s. | Triply coordinated oxygen ($V_3$-$O_C$) stretching mode. |
| 710 | $B_{2g}$, $B_{3g}$ | ν(V-O-V)s | Doubly coordinated oxygen ($V_2$-$O_B$) stretching mode. |

| | | | |
|---|---|---|---|
| 1006 | $A_g$ | ν(V=O)s | Stretching mode vibrations of the shortest vanadium oxygen bond $V=O_V$). |

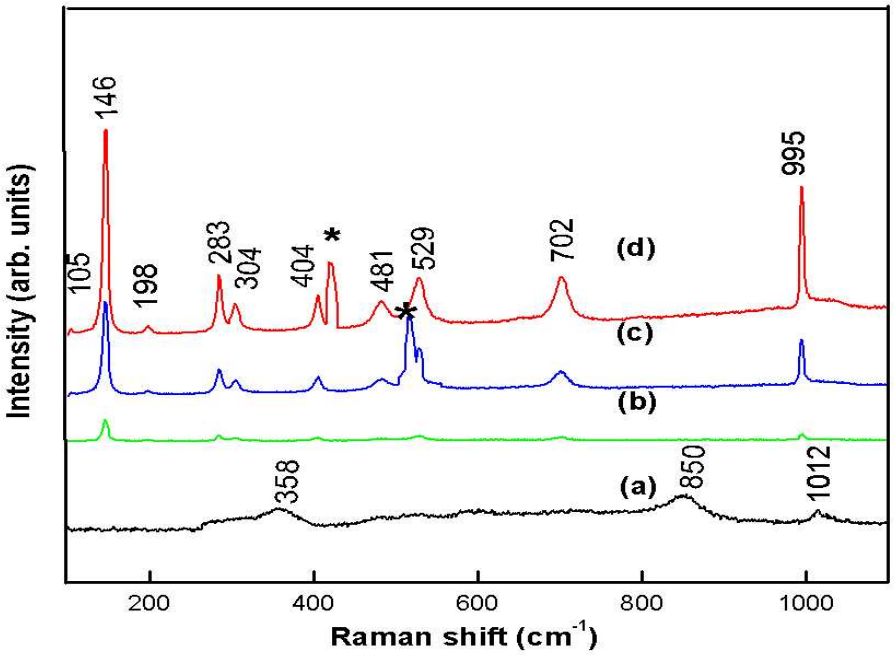


Figure 4:- Raman scattering spectra of (a) $V_2O_5$:G, (b) $V_2O_5$:Q, (c) $V_2O_5$:Si and (d) $V_2O_5$:A. The '*' indexed peaks corresponding to substrate.

### 3.5. Transport Measurements:

Temperature dependence of resistivity (ρ) of $V_2O_5$:G, $V_2O_5$:Q, $V_2O_5$: Si and $V_2O_5$:A thin films in the temperature range 300-400 K is shown in fig 5(a). All the samples show semiconducting behavior as electrical resistivity decreases with temperature. Further electrical resistivity decrease in the following order $V_2O_5$:G >$V_2O_5$:Q > $V_2O_5$:Si > $V_2O_5$:A. Hall measurements of samples demonstrate that all these films are n type semiconductors. Fig. 5 (B) displays variation of carrier density (n) and carrier mobility (μ) in the temperature range 300-400 K of the samples. Carrier concentration increases with temperature but the mobility decreases with temperature. Decrease in μ values may be caused by increase in carrier scattering due to thermal phonons. Comparison of n and μ of $V_2O_5$:G, $V_2O_5$:Q, $V_2O_5$:Si, and $V_2O_5$:A films demonstrate that carrier concentration increases in the following order $V_2O_5$:G >$V_2O_5$:Q > $V_2O_5$:Si > $V_2O_5$:A where as

mobility increases in the following order $V_2O_5$:Q, $V_2O_5$:Si, and $V_2O_5$:A to $V_2O_5$:G in the whole temperature range. Further the differences become more enhanced with temperature. Variation of resistivity, carrier concentration and mobility in these orders can be explained on the basis of thickness and crystallinity differences of the films. Both film thickness and crystallinity increases from $V_2O_5$:G to $V_2O_5$:Q to $V_2O_5$:Si to $V_2O_5$: A. As a film thickness decreases stacking defects increases and these defects trap the carriers and lower the free carrier concentration [46-47] and thus carrier concentration increases as we go from $V_2O_5$:G to $V_2O_5$:Q to $V_2O_5$:Si to $V_2O_5$:A. In additional film grown on glass substrate is amorphous in nature where as films deposited on alumina, silicon and quartz are crystalline in nature. The crystallites formed in $V_2O_5$:A, $V_2O_5$:Si and $V_2O_5$:Q produce a number of grain boundaries and these boundaries acts as scattering centers for the flow of charge carriers and thus cause reduction in the μ values as we go from amorphous film fabricated on glass to the crystalline films fabricated on alumina, silicon and quartz. Further as one goes from $V_2O_5$:A to $V_2O_5$:Si to $V_2O_5$:Q grain size decreases thus number of grain boundaries increases which results increase in carrier mobility from $V_2O_5$:A to $V_2O_5$:Si to $V_2O_5$:Q. Fig 5(C) displays Seebeck coefficient (s) of $V_2O_5$:G, $V_2O_5$:Q, $V_2O_5$: Si and $V_2O_5$:A thin films in the temperature range 300-400 K. Negative value of s also demonstrate that all films are n type semiconductors. The s value increases significantly over the entire temperature range from amorphous $V_2O_5$:G to crystalline $V_2O_5$:Q, $V_2O_5$:Si and $V_2O_5$:A thin films. The s value increases with decrease in crystallite size from $V_2O_5$:A to $V_2O_5$:Si to $V_2O_5$:Q. This can be understood as: the energy barrier formed at the grain boundaries acts as an additional trap centers and traps low energy charge carriers and this filtering of charge carriers by grain boundaries enhance average energy of carriers taking part in transport mechanism [48]. The value of thermoelectric power depends on the mean carrier energy relative to the Fermi level [49]. Therefore, this phenomenon of filtering of charge carriers also leads to increase in s value from $V_2O_5$:A, $V_2O_5$:Si, to $V_2O_5$:Q. Further with increase in temperature average energy of charge carriers taking part in transport mechanism increases, results an increase in s value with temperature.

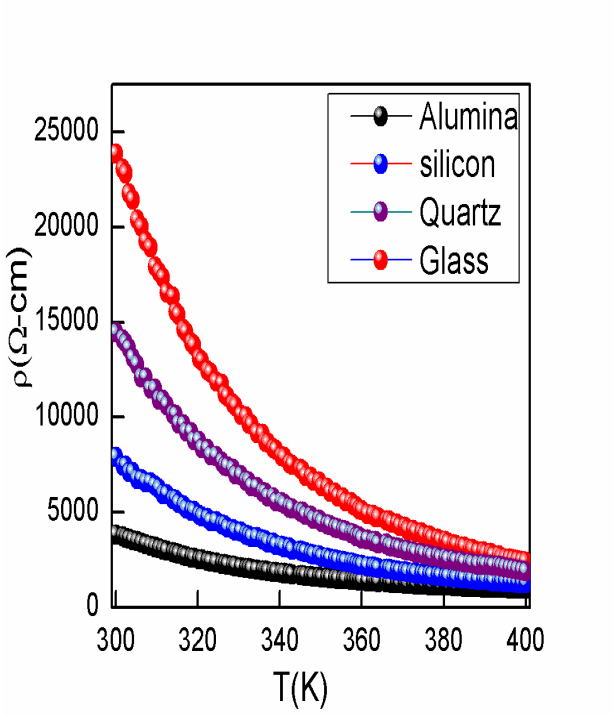


(a)

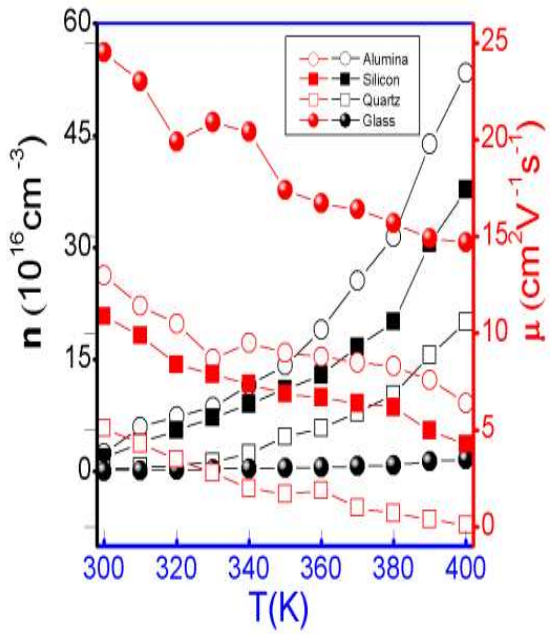


(b)

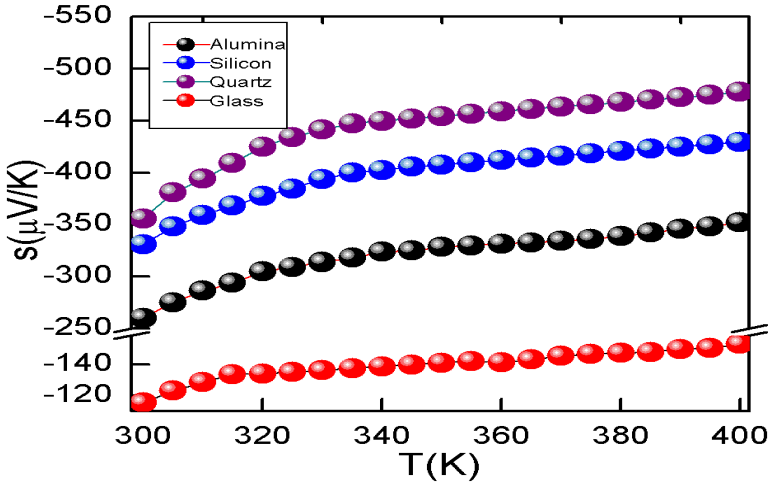


(c)

Figure 5:- (a) Electrical resistivity, (b) Carrier mobility and Concentration, and (c) seebeck coefficient of $V_2O_5$: Glass (b) $V_2O_5$:Q (c) $V_2O_5$: Si and (d) $V_2O_5$: Alumina thin films as a function of temperature.

## 4. Model for crystallization of $V_2O_5$ thin films on different substrates

Lattice mismatch between the substrates and the $V_2O_5$ and the underlying surface strongly affects nucleation and growth processes. In this section we model for the effect of substrates on the crystallization of $V_2O_5$ thin films. Figure (5) shows the schematic diagram of spherical

nuclei that nucleated on the hetero-substrate. The driving force for nucleation is Gibbs free energy [50,51]. The Gibbs free energy change for the nucleation of spherical nuclei of radius r on the hetero-substrate [50] is given by.

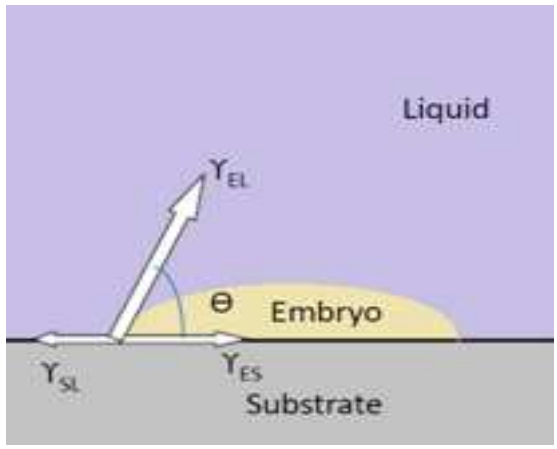


Figure 6:- Schematic diagram displaying the spherical nuclei nucleated on the hetero-substrate.

$$\Delta G_{Het.} = -V.\Delta G_v + \sum A_j \gamma_j \quad (3)$$

$$= -V.\Delta G_v + (A_{EL}\gamma_{EL} + A_{ES}\gamma_{ES} - A_{SL}\gamma_{SL}) \quad (4)$$

$$= -V.\Delta G_v + \Delta G_S \quad (5)$$

Where V is the volume of the spherical cluster, $\Delta G_v$ the Gibbs free energy of molar volume, $A_{EL}$ and $\gamma_{EL}$ the interface area and the interface energy of embryo-liquid interface, $A_{ES}$ and $\gamma_{ES}$ the interface area and the energy of embryo–substrate interface, and $A_{SL}$ and $\gamma_{SL}$ is the interface area and the energy between substrate-liquid interfaces. According to geometry

$$V = \frac{\pi r^3 (2+m)(1-m)^2}{3} \quad (6)$$

$$A_{SL} = 2\pi r^2 (1-m) \quad (7)$$

$$A_{HL} = \pi r^2 (1-m^2) \quad (8)$$

Where r is the radius of spherical cluster and m describes the interaction between liquid embryo and solid substrate and has been described in the classical model with the help of young equation [51].

$$m = \cos\theta = \frac{\gamma_{SL} - \gamma_{SE}}{\gamma_{EL}} \quad (9)$$

Where θ is the contact or wetting angle between the substrate and liquid embryo as shown in figure 5. Thus, we can obtain

$$\Delta G_{Het.} = \left(\frac{4}{3}\pi r^3 \Delta G_v + 4\pi r^2 \gamma_{SH}\right)\frac{(2+m)(1-m)^2}{4} \quad (10)$$

$$\Delta G_{Het.} = \left(\frac{4}{3}\pi r^3 \Delta G_v + 4\pi r^2 \gamma_{SH}\right) f(\theta) \quad (11)$$

Where the factor

$$f(\theta) = \frac{(2+m)(1-m)^2}{4} \quad (12)$$

is called heterogeneous factor, and its value lies in the range of 0-1. Its value is 1, when clusters nucleated on the homo-substrates. The critical nucleus radius, $r^*$, found by setting $\partial\Delta G/\partial r = 0$, with the result

$$r^* = -\frac{2\gamma_{SL}}{\Delta G_V} \quad (13)$$

It is important to note that the critical radius r* remains unchanged for heterogeneous nucleation and homogeneous nucleation. However, the volume (V) can be significantly less for heterogeneous nucleation due to the wetting angle affecting the shape of the nucleus. The associated energy barrier for nucleation is found by substituting $r^*$ in equation (8)

$$\Delta G^*_{Het.} = \frac{16}{3}\pi\frac{\gamma_{SL}^3}{(\Delta G)^2}\frac{(2+m)((1-m)^2}{2} \quad (14)$$

$$= \frac{16}{3}\pi\frac{\gamma_{SL}^3}{(\Delta G)^2}\frac{(2+\cos\theta)((1-\cos\theta)^2}{2} \quad (15)$$

$$= \frac{16}{3}\pi\frac{\gamma_{SL}^3}{(\Delta G)^2} f(\theta) \quad (16)$$

$$= \Delta G^*_{Homo.} f(\theta) \quad (17)$$

The nucleation rate J, which is the number of critical nuclei formed per unit time per unit volume is usually written in Arrhenius activation form as.

$$J = D\exp\left(-\frac{\Delta G^*}{K_B}\right) \quad (18)$$

Where D is a kinetic pre-exponential factor which is correlated to encounter frequency between the molecules and consequently dependent on their diffusion coefficients, $K_B$ is the Boltzmann constant, and $\Delta G^*$ is the reversible work of formation of critical nucleus. The diffusion coefficient D is observed to depend upon temperature as [52].

$$D = D_0\exp\left(-\frac{E_d}{K_B T}\right) \quad (19).$$

Where $E_d$ is the activation energy for diffusion, $K_B$ is the Boltzmann's constant, T is the absolute temperature, and $D_0$ is a temperature-independent factor which depends upon the choice of material and deposit. Equation (18) together with equation (17) and (19) defines the rate of heterogeneous nucleation of liquid embryos on the heterogeneous substrate. Thus rate of nucleation depends upon the nature of material of the substrate, temperature of substrate and the contact angle between substrate and liquid embryo. Hence maintaining all the substrates at fixed temperature during deposition of $V_2O_5$ and post annealed at same temperature, nucleation of $V_2O_5$ varies from substrate to substrate. The main parameter that may determine the growth of $V_2O_5$ thin film on a substrate at fixed temperature is the contact angle and this contact angle characterizes the interactions between the sol and substrate known as adhesive forces, measures the wettability of solid surface by liquid. The work of adhesion, $W_{ad}$, is defined as [53].

$$Wad = \sigma lv\,(1 + \cos\theta) \qquad (20)$$

A high work of adhesion indicates good wetting; whereas, a low work of adhesion indicates poor wetting. Fig 6 (a), (b), (c) and (d) show the wetting and spreading phenomena of water on glass, quartz, silicon, and alumina substrates respectively. Glass substrates are most wetted and alumina substrates are least wetted. Magnitude of contact angle increases from $19^0$ for glass to $35.4^0$ for quartz to $38.5^0$ for silicon to $46.5^0$ to alumina substrates. Similar trend of increase of contact angle from glass to quartz to silicon to alumina substrate is expected for $V_2O_5$ sol. This indicates that magnitude of adhesive forces between sol and substrate decreases from glass to quartz to Si to alumina substrate. Thus $V_2O_5$ sol spreads more on glass and least on alumina. As a consequence of this, nucleation barrier increases from glass to quartz to silicon to alumina as shown in Fig. (7) and thus the nucleation rate J, which is the number of critical nuclei formed per unit time per unit volume decreases from glass to quartz to Si to alumina substrate. Thus the number of critical nuclei that gets formed on the surface of the substrates decreases from glass to quartz to Si to alumina and hence the thickness and crystallinity of $V_2O_5$ thin film increases from glass to quartz to silicon to alumina substrate.

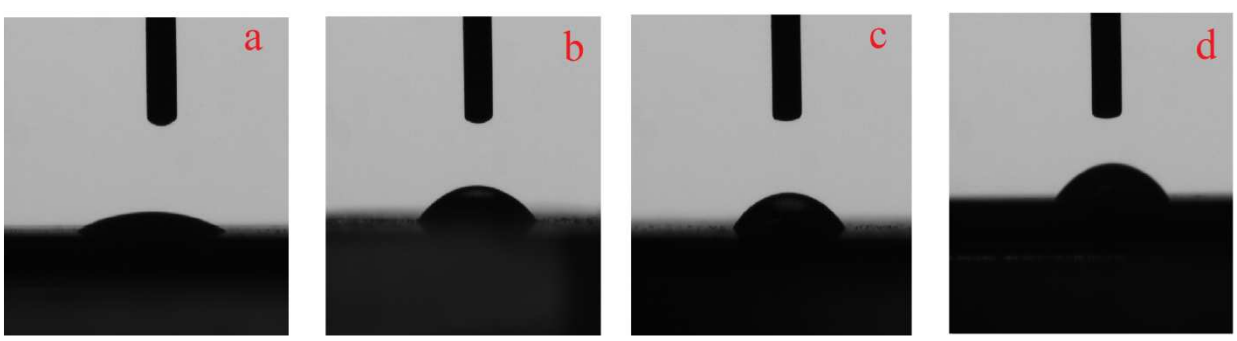


Fig. 6:- Images of water contact angle on (a) Glass, (b) Quartz, (c) Si and (d) Alumina substrates.

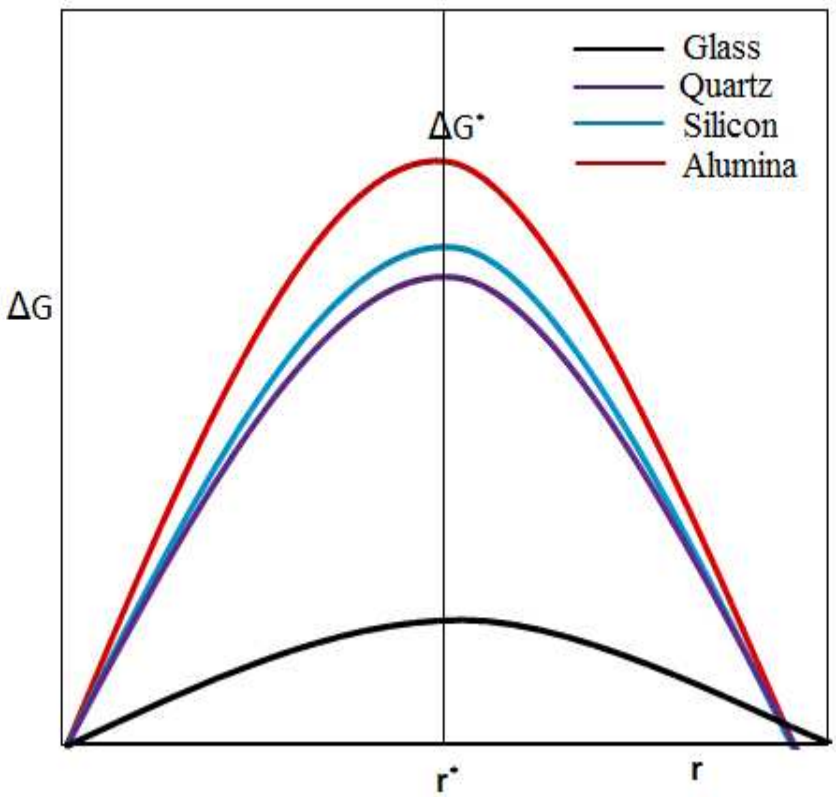


Fig. 7:- Schematic diagram showing variation of Gibbs free energy with radius of nuclei.

## 5. Conclusion

The nature of substrates determines the properties of $V_2O_5$ thin films. SEM images showed a change in surface morphology of $V_2O_5$ films from substrate to substrate. Films deposited on glass substrates are amorphous in nature with smooth surface, whereas films deposited on quartz, Si and alumina substrates are crystalline. Degree of crystallization increases from quartz to Si to alumina. RBS results show thickness of film increases from glass to quartz to silicon to alumina substrate. XRD and Raman results displays that films fabricated on glass substrate are amorphous in nature where as films fabricated on quartz, silicon, and alumina are crystalline and crystallinity increases from quartz to silicon to alumina. Basically these are the interactions between sol and substrate (adhesive forces) that plays significant role to elucidate the thickness and degree of crystallization of $V_2O_5$ thin films. As the magnitude of adhesive forces between sol and substrate increases, both film thickness and crystallinity enhances. Electrical and thermoelectrical properties were found to be functions of crystallization and thickness. As film

thickness and crystallization increases from $V_2O_5$:G to $V_2O_5$:Q to $V_2O_5$:Si to $V_2O_5$:A, both carrier concentration and conductivity increases. Carrier mobility decreases from amorphous film to crystalline film and increases with increasing crystallite size. Seebeck coefficient shows a strong dependence on crystallization. Seebeck coefficient increases from amorphous film to crystalline film and then decreases with increase in crystallite size. This behavior of μ and s with crystallization is due scattering and tapping of charge carriers along the grain boundaries and stacking defects.

**Acknowledgements:** One of the authors (B.A) acknowledges the director, NIT-Srinagar and Director, IUAC, New Delhi for their support and encouragements. He also thanks Materials Science group for all characterization facilities.

**References:-**

[1]. Darling, R. B., & Iwanaga, S. (2009). Structure, properties, and MEMS and microelectronic applications of vanadium oxides. *Sadhana*, *34*(4), 531-542.

[2]. Morin, F. J. (1959). Oxides which show a metal-to-insulator transition at the Neel temperature. *Physical Review Letters*, *3*(1), 34-36.

[3]. Smith, R. L., Rohrer, G. S., Lee, K. S., Seo, D. K., & Whangbo, M. H. (1996). A scanning probe microscopy study of the (001) surfaces of $V_2O_5$ and $V_6O_{13}$. *Surface science*, *367*(1), 87-95.

[4]. F. Hulliger, in *Structural Chemistry of Layer-Type Phases*, edited by F.Lévy _Reidel, Dordrecht, (1976), Fig. 100, with kind permission of Springer Science and Business Media.

[5]. Wang, Y., & Cao, G. (2006). Synthesis and enhanced intercalation properties of nanostructured vanadium oxides. *Chemistry of materials*,*18*(12), 2787-2804.

[6]. Petkov, V., et al. "Structure beyond Bragg: Study of $V_2O_5$ nanotubes."*Physical Review B* 69.8 (2004): 085410.

[7]. Kim, G. T., Muster, J., Krstic, V., Park, J. G., Park, Y. W., Roth, S., & Burghard, M. (2000). Field-effect transistor made of individual $V_2O_5$ nanofibers.*Applied Physics Letters*, *76*(14), 1875-1877.

[8]. Ramana, C. V., Smith, R. J., Hussain, O. M., Chusuei, C. C., & Julien, C. M. (2005). Correlation between growth conditions, microstructure, and optical properties in pulsed-laser-deposited $V_2O_5$ thin films. *Chemistry of materials*,*17*(5), 1213-1219.

[9]. Lu, Z., Levi, M. D., Salitra, G., Gofer, Y., Levi, E., & Aurbach, D. (2000). Basic electroanalytical characterization of lithium insertion into thin, well-crystallized $V_2O_5$ films. *Journal of Electroanalytical Chemistry*, *491*(1), 211-221.

[10]. West, K., Zachau-Christiansen, B., Skaarup, S. V., & Poulsen, F. W. (1992). Lithium insertion in sputtered vanadium oxide film. *Solid State Ionics*, *57*(1), 41-47.

[11]. Park, Y. J., Ryu, K. S., Kim, K. M., Park, N. G., Kang, M. G., & Chang, S. H. (2002). Electrochemical properties of vanadium oxide thin film deposited by RF sputtering. *Solid State Ionics*, *154*, 229-235.

[12]. Mui, S. C., Jasinski, J., Leppert, V. J., Mitome, M., Sadoway, D. R., & Mayes, A. M. (2006). Microstructure effects on the electrochemical kinetics of vanadium pentoxide thin-film cathodes. *Journal of The Electrochemical Society*, *153*(7), A1372-A1377.

[13]. Benayad A., Martinez H. , Gies A. Pecquenard B., Levasseur A.,. Gonbeau D. (2006). XPS investigations achieved on the first cycle of $V_2O_5$ thin films used in lithium microbatterie. *Journal of Electron Spectroscopy and Related Phenomena* ***150,*** *1-10*

[14]. Szörényi, T., Bali, K., & Hevesi, I. (1980). Structural characterization of amorphous vanadium pentoxide thin films prepared by chemical vapour deposition/CVD. *Journal of Non-Crystalline Solids*, *35*, 1245-1248.

[15]. Inumaru, K., Okuhara, T., Misono, M., Matsubayashi, N., Shimada, H., & Nishijima, A. (1992).EXAFS analysis of vanadium oxide thin overlayers on silica prepared by chemical vapour deposition. *J. Chem. Soc., Faraday Trans.*,*88*(4), 625-630.

[16]. Lindström, R., Maurice, V., Zanna, S., Klein, L., Groult, H., Perrigaud, L., Cohen, C.,& Marcus, P. (2006). Thin films of vanadium oxide grown on vanadium metal: oxidation conditions to produce $V_2O_5$ films for Li-intercalation applications and characterisation by XPS, AFM, RBS/NRA. *Surface and interface analysis*,*38*(1), 6-18.

[17]. Światowska-Mrowiecka, J., Maurice, V., Zanna, S., Klein, L., Briand, E., Vickridge, I., & Marcus, P. (2007). Ageing of $V_2O_5$ thin films induced by Li intercalation multi-cycling. *Journal of power sources*, *170*(1), 160-172.

[18]. Fang, G. J., Liu, Z. L., Wang, Y., Liu, Y. H., & Yao, K. L. (2001). Synthesis and structural, electrochromic characterization of pulsed laser deposited vanadium oxide thin films. *Journal of Vacuum Science & Technology A*, *19*(3), 887-892.

[19]. Mantoux, A., Groult, H., Balnois, E., Doppelt, P., & Gueroudji, L. (2004). Vanadium oxide films synthesized by CVD and used as positive electrodes in secondary lithium batteries. *Journal of The Electrochemical Society*, *151*(3), A368-A373.

[20]. Le, D. B., Passerini, S., Tipton, A. L., Owens, B. B., & Smyrl, W. H. (1995). Aerogels and xerogels of $V_2O_5$ as intercalation hosts. *Journal of The Electrochemical Society*, *142*(6), L102-L103.

[21]. Bouzidi, A., Benramdane, N., Nakrela, A., Mathieu, C., Khelifa, B., Desfeux, R., & Da Costa, A. (2002). First synthesis of vanadium oxide thin films by spray pyrolysis technique. *Materials Science and Engineering: B*, *95*(2), 141-147.

[22].Kang, M., Kim, I., Kim, S. W., Ryu, J. W., & Park, H. Y. (2011). Metal-insulator transition without structural phase transition in $V_2O_5$ film. *Applied Physics Letters*, *98*(13), 131907-131907.

[23].Blum, R. P., Niehus, H., Hucho, C., Fortrie, R., Ganduglia-Pirovano, M. V., Sauer, J., ... & Freund, H. J. (2007). Surface metal-insulator transition on a vanadium pentoxide (001) single crystal. *Physical review letters*, *99*(22), 226103.

[24].Pergament, A. L., Stefanovich, G. B., & Velichko, A. A. (2013). Oxide Electronics and Vanadium Dioxide Perspective: A Review.

[25].Ramana, C. V., Hussain, O. M., Naidu, B. S., & Reddy, P. J. (1997). Spectroscopic characterization of electron-beam evaporated $V_2O_5$ thin films. *Thin Solid Films*, *305*(1), 219-226.

[26]. Zhu, M., Zhang, Z., & Miao, W. (2006). Intense photoluminescence from amorphous tantalum oxide films. *Applied physics letters*, *89*(2), 021915-021915.

[27]. Losurdo, M., Bruno, G., Barreca, D., & Tondello, E. (2000). Dielectric function of $V_2O_5$ nanocrystalline films by spectroscopic ellipsometry: Characterization of microstructure. *Applied Physics Letters*, *77*(8), 1129-1131.

[28]. Kang, M. I., Kim, I. K., Oh, E. J., Kim, S. W., Ryu, J. W., & Park, H. Y. (2012). Dependence of optical properties of vanadium oxide films on crystallization and temperature. *Thin Solid Films*, *520*(6), 2368-2371.

[29].Santos, R., Loureiro, J., Nogueira, A., Elangovan, E., Pinto, J. V., Veiga, J. P., ... & Ferreira, I.(2013). Thermoelectric properties of V 2 O 5 thin films deposited by thermal evaporation. *Applied Surface Science*, *282*, 590-594.

[30]. Iwanaga, S., Marciniak, M., Darling, R. B., & Ohuchi, F. S. (2007). Thermopower and electrical conductivity of sodium-doped $V_2O_5$ thin films.*Journal of applied physics*, *101*(12), 123709.

[31]. Lazaro E., Bhamidipati M., Aldissi M., & Dixon B. (1998).Thermoelectric Organics, USAR Office, East Falmouth, Massachusetts, USA,.

[32]. Ren, X., Jiang, Y., Zhang, P., Liu, J., & Zhang, Q. (2009). Preparation and electrochemical properties of $V_2O_5$ submicron-belts synthesized by a sol–gel $H_2O_2$ route. *Journal of sol-gel science and technology*, *51*(2), 133-138.

[33]. Bachmann, H. G., Ahmed, F. R., & Barnes, W. H. (1961). The crystal structure of vanadium pentoxide. *Zeitschrift für Kristallographie-Crystalline Materials*,*115*(1-6), 110-131.

[34]. Hwang, K. S., Ahn, J. H., & Kim, B. H. (2006). Vanadium-doped nanocrystalline $TiO_2$ layer prepared by spin coating pyrolysis. *Journal of materials science*, *41*(10), 3151-3153.

[35]. Livage, J. (1991). Vanadium pentoxide gels. *Chemistry of Materials*, *3*(4), 578-593.

[36]. Brinker, C. J., & Scherer, G. W. (Eds.). (1990). *Sol-gel science: the physics and chemistry of solgel processing*. Gulf Professional Publishing.

[37]. Alonso, B., & Livage, J. (1999). Synthesis of Vanadium Oxide Gels from Peroxovanadic Acid Solutions: A51V NMR Study. *Journal of Solid State Chemistry*, *148*(1), 16-19

[38]. Ramana, C. V., Hussain, O. M., Naidu, B. S., & Reddy, P. J. (1997). Spectroscopic characterization of electron-beam evaporated $V_2O_5$ thin films. *Thin Solid Films*, *305*(1), 219-226.

[39]. Abello, L., Husson, E., Repelin, Y., & Lucazeau, G. (1983). Vibrational spectra and valence force field of crystalline V2O5. *Spectrochimica Acta Part A: Molecular Spectroscopy*, *39*(7), 641-651.

[40]. Haber, J., Witko, M., & Tokarz, R. (1997). Vanadium pentoxide I. Structures and properties. *Applied Catalysis A: General*, *157*(1), 3-22.

[41]. Beattie, I. R., & Gilson, T. R. (1969). Oxide phonon spectra. *Journal of the Chemical Society A: Inorganic, Physical, Theoretical*, 2322-2327.

[42]. Clauws, P., Broeckx, J., & Vennik, J. (1985). Lattice Vibrations of $V_2O_5$. Calculation of Normal Vibrations in a Urey-Bradley Force Field. *physica status solidi (b)*, *131*(2), 459-473.

[43]. Lee, S. H., Cheong, H. M., Seong, M. J., Liu, P., Tracy, C. E., Mascarenhas, A., ... & Deb, S. K. (2003). Raman spectroscopic studies of amorphous vanadium oxide thin films. *Solid State Ionics*, *165*(1), 111-116.

[44]. Abello, L., Husson, E., Repelin, Y., & Lucazeau, G. (1983). Vibrational spectra and valence force field of crystalline V2O5 *Spectrochimica Acta Part A: Molecular Spectroscopy*, *39*(7), 641-651.

[45]. Fang, G. J., Liu, Z. L., Wang, Y. Q., Liu, H. H., & Yao, K. L. (2000). Orientated growth of $V_2O_5$ electrochromic thin films on transparent conductive glass by pulsed excimer laser ablation technique. *Journal of Physics D: Applied Physics*, *33*(23), 3018.

[46].Lin, S. S., Huang, J. L., & Lii, D. F. (2005). The effect of thickness on the properties of Ti-doped ZnO films by simultaneous rf and dc magnetron sputtering. *Surface and Coatings Technology*, *190*(2), 372-377.

[47].Qu, Y., Gessert, T. A., Ramanathan, K., Dhere, R. G., Noufi, R., & Coutts, T. J. (1993). Electrical and optical properties of ion beam sputtered ZnO: Al films as a function of film thickness. *Journal of Vacuum Science & Technology A*,*11*(4), 996-1000.

[48]. Bala, M., Gupta, S., Tripathi, T. S., Varma, S., Tripathi, S. K., Asokan, K., & Avasthi, D. K. (2015). Enhancement of thermoelectric power of PbTe: Ag nanocomposite thin films. *RSC Advances*, *5*(33), 25887-25895.

[49]. Martin, J., Wang, L., Chen, L., & Nolas, G. S. (2009). Enhanced Seebeck coefficient through energy-barrier scattering in PbTe nanocomposites.*Physical Review B*, *79*(11), 115311

[50]. Yang, G. W., & Liu, B. X. (2000). Nucleation thermodynamics of quantum-dot formation in Vgroove structures. *Physical Review B*, *61*(7), 4500.

[51]. Kwok, D. Y., Lam, C. N. C., Li, A., Leung, A., Wu, R., Mok, E., & Neumann, A. W. (1998). Measuring and interpreting contact angles: a complex issue.*Colloids and Surfaces A: Physicochemical and Engineering Aspects*, *142*(2), 219-235.

[52]. Kittel, C. (1968). *Introduction to solid state physics*. New York: Wiley.

[53]. Neumann A.W, and Good. R.J, *Surface and Colloid Science,* vol. II, ed. Good R.J. and Stromberg. R.R. (New York: Plenum Press, 1979).